

Monopile rotation under complex cyclic lateral loading in sand

IONA A. RICHARDS*, BYRON W. BYRNE† and GUY T. HOULSBY‡

Monopiles supporting offshore wind turbines experience combined moment and horizontal loading which is both cyclic and complex – continuously varying in amplitude, direction and frequency. The accumulation of rotation with cyclic loading (ratcheting) is a key concern for monopile designers and has been explored in previous experimental studies, where constant-amplitude cyclic tests have shown rotation to accumulate as a power-law with cycle number. This paper presents results from laboratory tests in dry sand, which explore the rotation response to constant and variable amplitude, unidirectional and multidirectional cyclic loading. The tests are designed to inform model development and provide insight into key issues relevant to monopile design. Unidirectional tests show behaviour consistent with previous studies and provide a basis for interpreting more complex tests; multidirectional tests provide new insight into the monopile response to multidirectional cyclic loading; and multi-amplitude storm tests highlight salient features of the response to realistic loading. Tests are conducted in both very loose and dense sand, where the behaviour is found to be qualitatively similar.

KEYWORDS: laboratory tests; piles & piling; repeated loading; sands; soil/structure interaction

INTRODUCTION

The vast majority of offshore wind turbines (OWTs) are supported on monopile foundations; in Europe monopiles represent 87% of all installed OWT foundations (Wind Europe, 2018). The monopile's prevalence is largely due to their simple design, robust installation procedures and established supply chain. These large-diameter open-ended steel piles have increased in size over time to support larger OWTs, and in deeper water, as the industry has matured. Modern monopiles have diameters up to 8 m (Sørensen *et al.*, 2017) with length (L) to diameter (D) ratios (L/D) of 3–6 (Schroeder *et al.*, 2015; Sørensen *et al.*, 2017); next-generation monopiles might be 10 m in diameter. The OWT structure is exposed to significant lateral loads caused by a combination of wind, waves and current. The resultant combined moment and horizontal loads experienced by the monopile are cyclic and complex, varying continuously in amplitude, direction and frequency.

The recent PISA project focused on understanding, and developing better methods to predict, the monopile's response to monotonic lateral loading, which is necessary for ultimate limit state (ULS) design and provides initial stiffness values for initial natural frequency calculations (Byrne *et al.*, 2017). This work demonstrated the inherent conservatism embedded in design guidelines originally developed for slender piles used in the offshore oil and gas industry (e.g. API, 2011; DNV GL, 2016), and should enable

the design of more efficient monopiles. However, as conservatism in ULS design is reduced, and as the magnitude of cyclic lateral loads increase with increasing monopile diameter, increasing water depth and increasing turbine size, design for cyclic lateral loading becomes more important. Turbine manufacturers typically specify strict tolerances on OWT structure rotation over their lifetime, and accumulation of foundation rotation due to cyclic loading (ratcheting) is a key concern.

Many previous experimental studies have explored the monopile response to cyclic lateral loading in sands, providing valuable insight. Most studies have focused on the monopile rotation response under constant-amplitude, unidirectional cyclic loading, with studies performed at both 1g (e.g. Leblanc *et al.*, 2010a; Nicolai & Ibsen, 2014; Arshad & Kelly, 2017) and in the centrifuge (e.g. Klinkvort & Hededal, 2013; Truong *et al.*, 2019). The monopile response to fan-type multidirectional loading has also been explored at 1g (Dührkop & Grabe, 2008; Rudolph & Grabe, 2013) and in the centrifuge (Rudolph *et al.*, 2014a), where multidirectional loading was found to be more damaging than unidirectional loading.

Monopile rotation has typically been found to evolve as a power-law with cycle number, and empirical relationships have been widely used to capture this behaviour (Leblanc *et al.*, 2010a; Klinkvort & Hededal, 2013). Achmus *et al.* (2009) incorporated a semi-empirical power-law expression into an elasto-plastic soil model to allow numerical calculation of monopile displacement, and this method has been shown to predict the results of Leblanc *et al.* (2010a) with reasonable accuracy. Meanwhile, Bayton *et al.* (2018) used centrifuge testing to develop contour diagrams, following the Norwegian Geotechnical Institute (NGI) cyclic degradation approach (Andersen, 2015), which allow prediction of a monopile's response to multi-amplitude cyclic loading. Linear superposition methods have also been adopted for multi-amplitude loading (Leblanc *et al.*, 2010b).

Although empirical methods and the cyclic degradation approach provide insight into the monopile's response to cyclic lateral loading and may be useful for initial design, they are not well adapted for prediction of the monopile response to the complex cyclic loading that would be

Manuscript received 12 November 2018; revised manuscript accepted 22 August 2019. Published online ahead of print 26 September 2019.

Discussion on this paper closes on 1 February 2021, for further details see p. ii.

Published with permission by the ICE under the CC-BY 4.0 license. (<http://creativecommons.org/licenses/by/4.0/>)

* Department of Engineering Science, Oxford University, Oxford, UK (Orcid:0000-0003-4241-6031).

† Department of Engineering Science, Oxford University, Oxford, UK (Orcid:0000-0002-9704-0767).

‡ Department of Engineering Science, Oxford University, Oxford, UK (Orcid:0000-0001-5807-8781).

experienced in the field. For example, it is not clear how these methods can account for the impact of multi-amplitude load order, which appears to be significant, particularly when load amplitude and average load varies between load packets (Truong *et al.*, 2019), and adaptation for multidirectional loading is likely to be challenging.

Models based on multi-surface plasticity are able to capture hysteretic behaviour, can respond to any arbitrary load history and can be adapted for multidimensional loading. Page *et al.* (2018) developed a multi-surface macro element for application to monopiles in clays, while Houlsby *et al.* (2017) developed a flexible multi-surface model supplemented with a ratcheting component (hyper-plastic accelerated ratcheting model (HARM)). HARM has been shown to predict the response of a monopile to constant and multi-amplitude cyclic loading at both model scale (Abadie *et al.*, 2019a) and large scale (Beuckelaers, 2017). However, validation of the performance of HARM under complex loading, and development of the calibration procedure for full-scale design, is necessary.

This paper explores the response of a monopile to unidirectional, multidirectional and multi-amplitude storm-type cyclic loading through $1g$ model tests. These tests provide insight into the monopile's response to complex cyclic loading, and have been designed to facilitate development of models in the HARM framework. The unidirectional tests add to the growing database of similar tests performed at $1g$ and in a centrifuge, demonstrating consistent behaviour, providing a basis for understanding the response to more complex loading, and later informing model calibration. The multidirectional cyclic response is then explored through perpendicular and radially spread (fan-type) loading tests. These constant-amplitude tests are not intended to be completely realistic, but instead provide insight into the monopile's fundamental multidirectional behaviour and can inform multidirectional model development. Finally, multi-amplitude, unidirectional and multidirectional storm-type loading is applied to the model monopile. These tests begin to show how behaviour observed in contrived laboratory tests may translate to behaviour under realistic cyclic loading; these tests may also be useful for model validation.

Several important phenomena occur during cyclic loading. Alongside ratcheting of the monopile, evolution of cyclic stiffness and hysteretic damping with cycles has been observed (Leblanc *et al.*, 2010a; Klinkvort & Heddal, 2013; Abadie *et al.*, 2019b), which is of concern for foundation designers. The response of a monopile to a single large load following cycling is also an important concern. However, this paper focuses primarily on the important phenomenon of evolution of monopile rotation, or 'ratcheting', under many cycles.

LABORATORY-SCALE TESTS

Laboratory set-up

Figure 1 shows the laboratory apparatus used to investigate the response of a model monopile to cyclic lateral loading. A rigid, hollow aluminium pile was used, at approximately 1:100 scale, with diameter $D = 80$ mm, wall thickness $t = 5$ mm and an embedded length $L = 320$ mm ($L/D = 4$). The pile is classified as smooth (average surface roughness, $R_a = 0.6 \mu\text{m}$) in contrast to typically rough full-scale monopiles; however, surface roughness has been shown to have only a small impact on the monopile's lateral response (Klinkvort, 2012). Following sand sample preparation, the pile was driven to the target embedment manually using a gravity hammer with drop height 300 mm and mass 1.4 kg and 2.8 kg for very loose and dense samples, respectively.

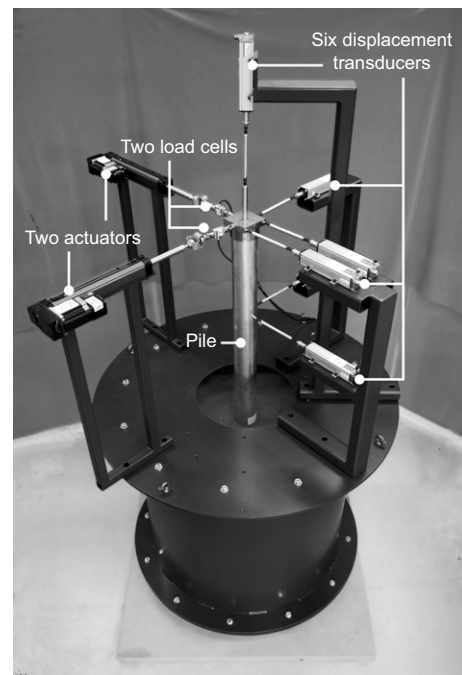


Fig. 1. Laboratory apparatus

Continually varying, multidirectional lateral load can be applied under load control with two electric actuators at a fixed eccentricity of $h = 800$ mm ($h/L = 2.5$), while six displacement transducers allow resolution of the monopile's position in six degrees of freedom. Further details on the apparatus design and associated software can be found in the paper by Richards *et al.* (2018).

Sand sample

The sand sample was prepared in a cylindrical tank with internal diameter 800 mm ($10D$) and height 800 mm, chosen to be practical while introducing minimal boundary effects, in line with, for example, the numerical investigation of Achmus *et al.* (2007). Yellow Leighton Buzzard 14/25 sand, with properties summarised in Table 1, was used for the tests presented here. Tests were conducted at two sand densities, and all tests were in dry sand to model fully drained conditions. Very loose samples were prepared by manual pouring from a very low drop height to achieve a unit weight of $\gamma' = 14.46 \text{ kN/m}^3 \pm 0.6\%$, corresponding to a relative density $R_D = 1\%$. Dense samples were prepared by air pluviation with a purpose-built sand-raining apparatus, achieving a unit weight of $\gamma' = 16.20 \text{ kN/m}^3 \pm 0.4\%$, corresponding to a relative density $R_D = 60\%$. Conical depressions with diameter around $2D$ were observed following pile installation at both densities, indicative of some local densification. The stated relative densities must therefore be considered pre-installation values.

The interaction between stress level, relative density and friction angle is important for laboratory-scale tests. Given the lower stress level at model scale, the sand relative density should be reduced to better approximate dilation and friction angles at full scale, where the stress level is higher (Bolton, 1986, 1987; Altaee & Fellenius, 1994). The relationship presented by Bolton (1986) is commonly used to calculate corresponding model- and full-scale relative densities (Leblanc *et al.*, 2010a; Zhu *et al.*, 2017). However, there are limited data supporting the proposed relationship of Bolton (1986) at very low stress levels, and the relationship was subsequently modified (Bolton, 1987) to limit dilatant behaviour at very low stress levels.

Table 1. Yellow Leighton Buzzard 14/25 sand properties

Particle sizes: mm	$D_{10}, D_{30}, D_{50}, D_{60}$	0.56, 0.69, 0.81, 0.87
Maximum unit weight: kN/m ³	γ'_{MAX}	17.64
Minimum unit weight: kN/m ³	γ'_{MIN}	14.43
Critical friction angle (Schnaid, 1990): degrees	ϕ'_{cr}	34.3

Table 2. Relative densities at model scale and full scale

Model-scale R_D : %	Lower estimate full-scale R_D : % (Bolton, 1987)	Upper estimate full-scale R_D : % (Bolton, 1986)	Classification at full scale
1.0	1.1	1.1	Very loose
60	65	115	Dense to very dense

The dilatant behaviour of sands at very low stress levels is still relatively poorly understood. Therefore, the relations from Bolton (1986, 1987) are used to provide upper and lower estimates, respectively, of the full-scale relative densities equivalent to the laboratory tests. Using equations (16) and (14) from Bolton (1986), and using the updated equation for relative dilatancy index presented by Bolton (1987), expressions for friction angle ϕ'_b at model-scale and full-scale representative stress levels are equated and solved for full-scale relative density. The vertical effective stress at 70% pile embedment ($\sigma'_v = 0.7\gamma' L$) is chosen as the representative stress.

Table 2 shows how the very loose sample at model scale unambiguously represents a very loose sample at full scale; however, Bolton's two methods give a wide range for the equivalent dense sample at full scale ($65 \leq R_D \leq 115\%$). The equivalent full-scale density could only be resolved with further research into sand behaviour at very low stress levels, specifically examining the variation of dilatancy with stress level, as reported by, for example, Lauder & Brown (2014). Here, the exact equivalent full-scale density for the denser sample is left open, and referred to as 'dense' throughout.

Scaling and normalisation

Leblanc *et al.* (2010a) derived a dimensionless framework for laterally loaded monopiles, incorporating an established relationship between shear modulus and stress level. Table 3 presents the key dimensionless parameters which can be used to translate between model scale and full scale. However, to facilitate comparison of results in very loose and dense sands it is more useful to normalise the data by moment and rotation reference values (M_R, θ_R). Typically monopiles in sand do not reach well-defined failure, and instead show continued hardening to large rotations. It is therefore necessary to (arbitrarily) define a reference rotation or displacement value, from which a reference load value can

be determined. A variety of different reference rotation and displacement values have been used by previous researchers in this area; for example, Leblanc *et al.* (2010a) use a dimensionless rotation of 4°, Abadie (2015) uses pile ground level displacement of 0.1D at model scale, Arshad & O'Kelly (2017) use a rotation of 1.5° at model scale, while Bayton *et al.* (2018) define a reference rotation of 0.25° on unloading to correspond to the serviceability limit state suggested by DNV GL (2016). In this work a reference rotation $\theta_R = 2^\circ$ at model scale is defined, broadly consistent with Abadie (2015) and Arshad & O'Kelly (2017). According to the dimensionless framework of Table 3, this corresponds to a larger reference rotation at full scale; however, the results could be recast with different reference values if required.

Monotonic response

The monotonic response of the monopile is an essential reference point for the cyclic behaviour and must be established first. Fig. 2(a) shows the average monotonic response from three pile tests at each density, while Figs 2(b) and 2(c) show the normalised average monotonic response, with upper- and lower-bound responses shown dashed. For the very loose sample, the tests were conducted in three different directions to check the invariance of the apparatus to load direction. Taking $\theta_R = 2^\circ$ gives projected values of $M_R = 26$ Nm for the very loose sample and of $M_R = 95$ Nm for the dense sample. Rate effects were investigated for loading rates between 0.08 and 0.8 Nm/s for the very loose sample, and found to be negligible.

Cyclic definitions

Figure 3 shows a schematic representation of the cyclic loading response. Rotation per cycle is defined at the average cyclic load magnitude ($M_{AV} = 1/2(M_{MIN} + M_{MAX})$), as the mean of the rotation value on reload and unload, indicated by points 'a' and 'b' respectively. For constant-amplitude loading, M_{AV} is constant, whereas for multi-amplitude loading M_{AV} varies with each reload or unload half-cycle (e.g. $M_{R,AV,n}, M_{U,AV,n}$). For both cases the total mean rotation at cycle n becomes

$$\theta_{M_n} = \frac{1}{2}(\theta_{a_n} + \theta_{b_n}) \quad (1)$$

Cycle 0 is defined for constant-amplitude loading as the first load-unload cycle, corresponding to the undisturbed response. With cycle 0 defined, the accumulated mean rotation at cycle n is

$$\Delta\theta_{M_n} = \theta_{M_n} - \theta_{M_0} \quad (2)$$

Table 3. Key dimensionless parameters (Leblanc *et al.*, 2010a)

Horizontal force	$\tilde{H} = \frac{H}{L^2 D \gamma'}$
Moment	$\tilde{M} = \frac{M}{L^3 D \gamma'}$
Rotation	$\tilde{\theta} = \theta \sqrt{\frac{p_a}{L \gamma'}}$
Eccentricity	$\tilde{e} = \frac{h}{L}$

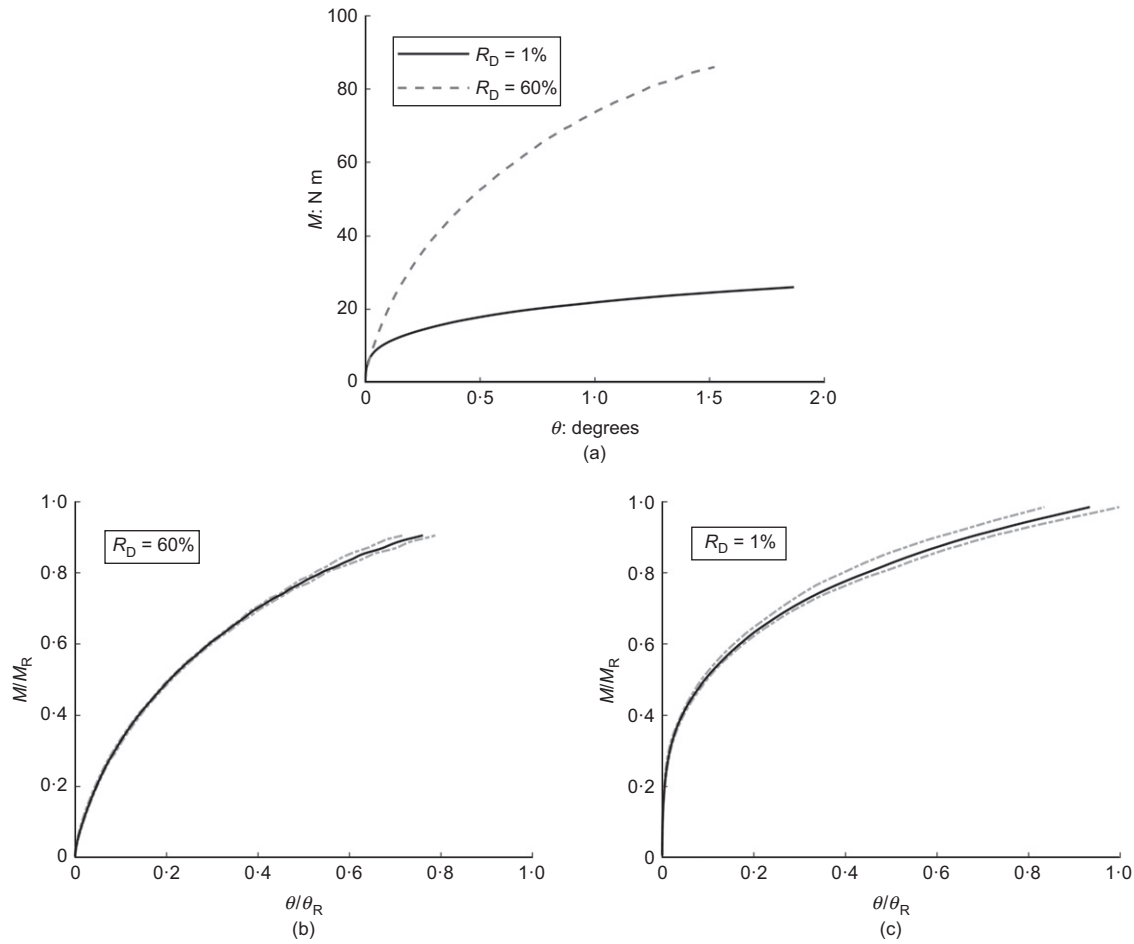


Fig. 2. Monotonic response: (a) average monotonic response; (b) normalised monotonic response in very loose sand; (c) normalised monotonic response in dense sand

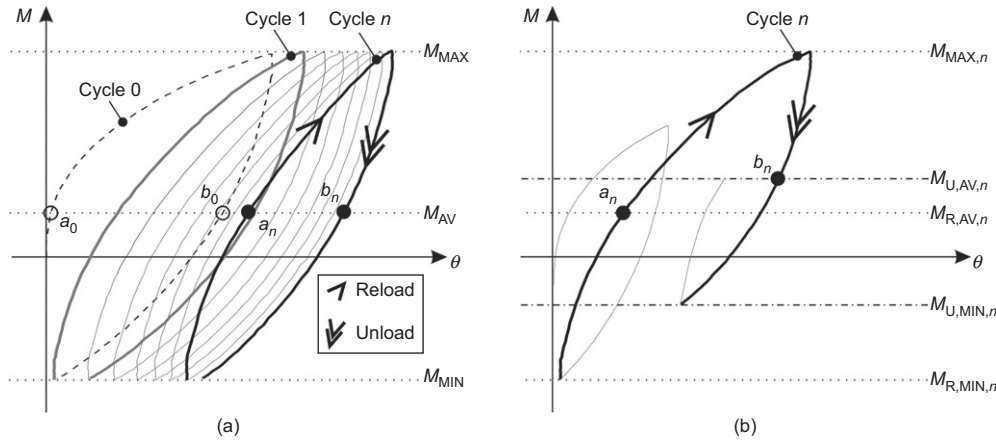


Fig. 3. Cyclic response definition: (a) constant-amplitude; (b) multi-amplitude

Accumulated rotation is useful for interpreting constant-amplitude tests, where it provides information about the evolution of rotation caused solely by cyclic loading.

This rotation definition has been selected so that the effect of ratcheting is not conflated with stiffening, softening or change in hysteresis loop shape. This definition is also aligned with the typical definition of strain per cycle used in element testing (the value of strain at average stress on reloading) (e.g. Andersen, 2015).

As described by Leblanc *et al.* (2010a), the cyclic loading is characterised by ζ_c and ζ_b

$$\zeta_c = \frac{M_{MIN}}{M_{MAX}} \quad (3)$$

$$\zeta_b = \frac{M_{MAX}}{M_R} \quad (4)$$

ζ_c characterises the load symmetry ($\zeta_c = 0$ for one-way loading, $\zeta_c = -1$ for symmetric two-way loading and $\zeta_c = 1$

for constant loading), while ζ_b and ζ_c together describe the load amplitude, relative to the reference moment M_R . The average load amplitude M_{AV} and cyclic load amplitude $M_{CYC} = 1/2(M_{MAX} - M_{MIN})$ are also important in controlling the cyclic response.

UNIDIRECTIONAL CONSTANT-AMPLITUDE CYCLIC RESPONSE

Table 4 summarises the unidirectional constant-amplitude tests presented in this paper. Sinusoidal cyclic loading was applied for all constant-amplitude cyclic tests. Both one-way

($\zeta_c = 0$) and partial two-way ($-1 < \zeta_c < 0$) tests were performed. The partial two-way tests were focused near $\zeta_c = -0.6$, as a number of studies at 1g have reported a maximum increase in ratcheting for this load condition (Leblanc *et al.*, 2010a; Zhu *et al.*, 2013; Nicolai & Ibsen, 2014; Albiker *et al.*, 2017). The ζ_b values were chosen to be as small as possible, while still allowing accurate application of load and resolution of the pile's full cyclic rotation response with the apparatus presented. Unidirectional, one-way tests were conducted to 10 000 cycles. Other tests were conducted to 1000 cycles as the ratcheting behaviour evolves logarithmically and there are diminishing returns associated with performing longer-term tests.

Figure 4 presents the monopile's ratcheting response for the tests presented in Table 4. The impact of ζ_c on the ratcheting response is clear, impacting both the magnitude of rotation and the shape of the evolution of rotation with cycle number in both the very loose and dense samples. For example, for the very loose sample with loading at $\zeta_b = 0.4$, the accumulated pile rotation at the 1000th cycle is 2.5 times larger when $\zeta_c = -0.6$, compared to $\zeta_c = 0$.

Two different empirical approaches are followed to consider the impact of ζ_c on the ratcheting response, both of which assume a power-law fit for evolution of the chosen strain variable ε with cycle number N

$$\varepsilon = AN^\alpha \quad (5)$$

The empirical framework of Leblanc *et al.* (2010a) assumes a constant exponent α , while Truong *et al.* (2019) let α vary with relative density R_D and load type ζ_c .

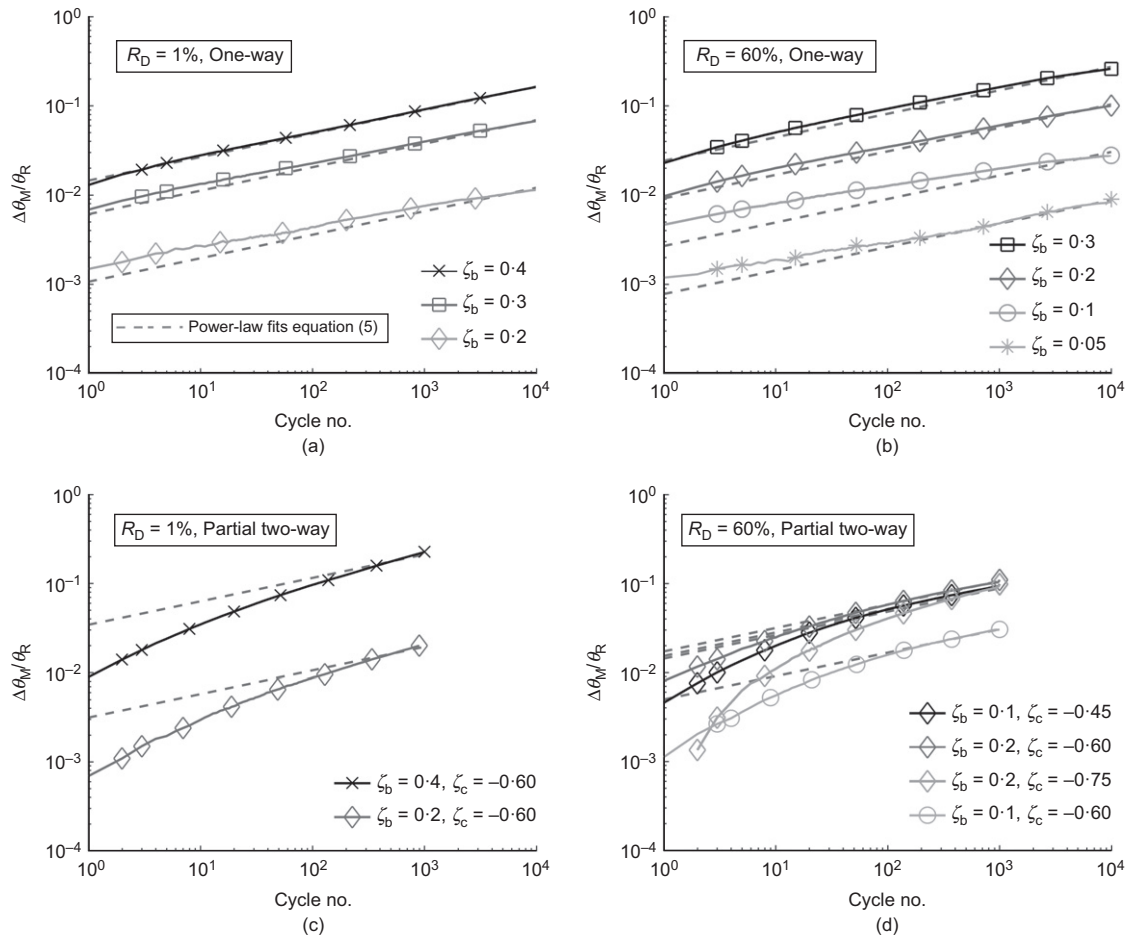


Fig. 4. Ratcheting response under unidirectional constant amplitude cyclic loading: (a) very loose sample, one-way cycling; (b) dense sample, one-way cycling; (c) very loose sample, partial two-way cycling; (d) dense sample, partial two-way cycling

Following Leblanc *et al.* (2010a), the dashed lines in Fig. 4 show the result of fitting equation (5) to all unidirectional constant-amplitude tests with equal weighting, assuming a common exponent α_c . A good fit is obtained to the one-way data and to the partial two-way data for $N > 100$, and there is no clear impact of load amplitude on goodness of fit. With the strain variable chosen here, $\Delta\theta_M$, the common exponent $\alpha_c = 0.26$. However, if the accumulated rotation at cycle peak ($\Delta\theta_p$) is used as the strain variable, consistent with previous work, then $\alpha = 0.30$, aligned with Leblanc *et al.* (2010a) and Abadie (2015).

In the approach of Leblanc *et al.* (2010a), the coefficient A is expressed as the product of two independent parameters, $A = T_c T_b$, where $T_c = f(\zeta_c)$ and $T_b = f(\zeta_b, R_D)$. The impact of ζ_c on ratcheting behaviour is therefore entirely characterised by T_c . Fig. 5 compares the T_c values obtained in this work to other studies, with tests conducted to a range of cycle numbers, $1000 < N < 100\,000$. Despite some scatter, there is a clear trend for increased T_c , and therefore increased ratcheting, for partial two-way loading at $\zeta_c \sim -0.6$. The highest T_c values occur for very loose sand samples. It should be noted that the choice of strain variable impacts the T_c values obtained, and the choice of accumulated or total strain is particularly significant (Albiker *et al.*, 2017). However, all studies presented in Fig. 5 use an accumulated rotation value ($\Delta\theta$) as the strain variable.

An alternative approach for assessing the impact of ζ_c on ratcheting behaviour is to let α vary with ζ_c , following the approach of Truong *et al.* (2019). To assess the variability of exponent α for the tests in this study, equation (5) is fitted to each individual unidirectional constant-amplitude test to obtain α . Fig. 6 shows how α has some dependency on ζ_c : increasing with decreasing ζ_c for $-0.75 < \zeta_c < 0$. A small dependency on R_D may also be seen, with higher α values for the looser sample. These trends are broadly in agreement with Truong *et al.* (2019).

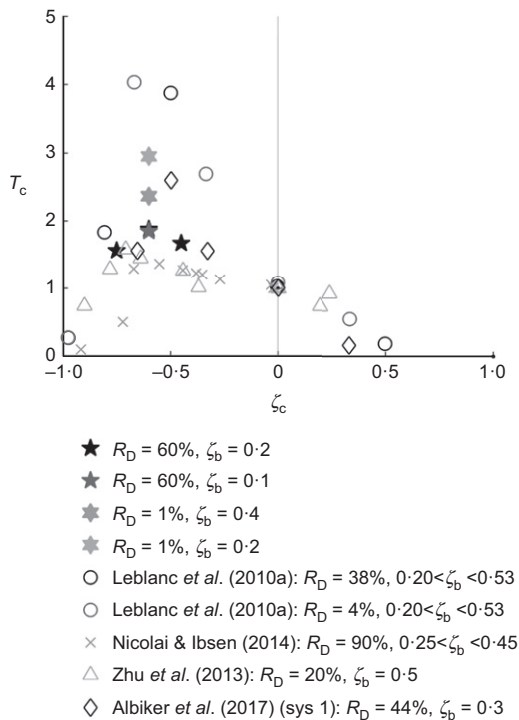


Fig. 5. Variation of T_c with ζ_c , following the empirical approach of Leblanc *et al.* (2010a)

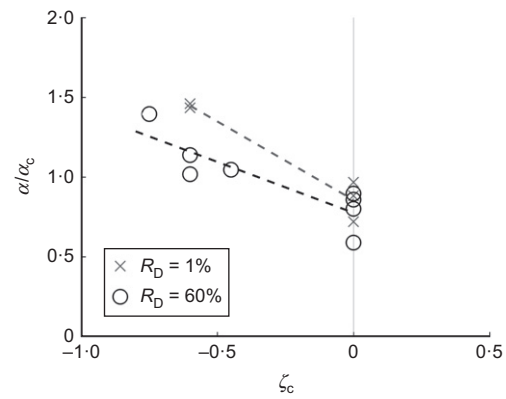


Fig. 6. Variation of α with ζ_c , following the empirical approach of Truong *et al.* (2019)

Both interpretations of the test results (Figs 5 and 6) demonstrate the importance of load asymmetry in controlling the ratcheting behaviour, and this must be accounted for in design methods. Qualitatively, the impact of ζ_c on ratcheting may be understood as a competition between (a) an increasing cyclic amplitude with increasingly negative ζ_c , which increases pile movement and therefore soil particle movement, and (b) a decreasing mean load with increasingly negative ζ_c . Increased particle movement is likely to increase ratcheting, which has been observed to occur through a convective mechanism (Cuéllar, 2011; Nicolai, 2017), while reducing the mean load will reduce ratcheting behaviour as the mechanism becomes more symmetric.

MULTIDIRECTIONAL CONSTANT-AMPLITUDE CYCLIC RESPONSE

In practice, monopiles are subjected to complex multidirectional loading as the wind and wave directions continually vary; Fig. 7 shows the spatial variation of wind and waves for an example site offshore the Netherlands (Bierbooms, 2003). Fan-type tests allow systematic investigation of the impact of spread angle (variation in loading direction) and closely follow tests performed by Dührkop & Grabe (2008), Rudolph & Grabe (2013) and Rudolph *et al.* (2014a), while novel perpendicular loading

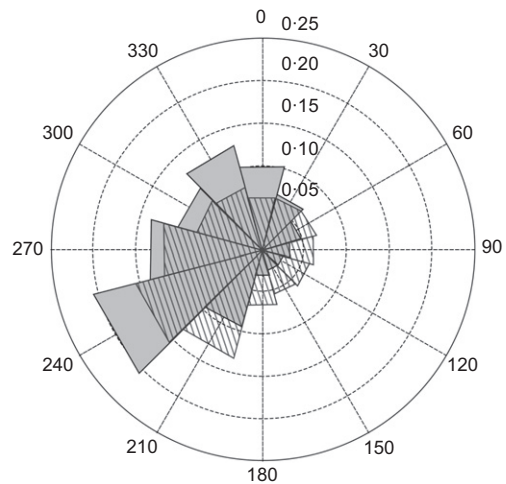


Fig. 7. Frequency of occurrence of wave direction (grey area) and wind direction (hashed area) for a site offshore the Netherlands. Modified from Bierbooms (2003)

Table 5. Perpendicular loading test series

Test name	Corresponding unidirectional test	Sand density	Load case	ζ_b	ζ_c	Cycles, N
L.X1	L.C3	Very loose	T-shape	0.2 in M_I , 0.2 in M_{II}	1 in M_I , -1 in M_{II}	1000
L.X2	L.C3	Very loose	L-shape	0.2 in M_I , 0.4 in M_{II}	1 in M_I , 0 in M_{II}	1000
D.X1	D.C3	Dense	T-shape	0.1 in M_I , 0.1 in M_{II}	1 in M_I , -1 in M_{II}	1000
D.X2	D.C3	Dense	L-shape	0.1 in M_I , 0.2 in M_{II}	1 in M_I , 0 in M_{II}	1000

tests provide fundamental insight into the multidirectional response.

Perpendicular loading

Table 5 and Fig. 8 summarise the perpendicular cyclic loading tests performed. These novel tests provide fundamental insight and may also represent misaligned wind and wave loading, which is common at some sites (Van Vledder, 2013). To isolate the effect of load direction, perpendicular tests are performed at the same cyclic amplitude (M_{CYC}) and average load (M_{AV}) as the corresponding unidirectional test. The T-shape tests have average load perpendicular to the cyclic loading direction, while the L-shape tests have equal average load applied both perpendicular and aligned to the cyclic loading direction. Load is first increased to M_{AV} in the direction of constant load, and then held constant while cyclic loading is applied. The notation I and II refer to arbitrary perpendicular directions normal to the pile's vertical axis.

Figure 9 presents the monopile's continuous total rotation response for the perpendicular loading tests, alongside the corresponding unidirectional tests. In all cases, ratcheting is mostly aligned with the direction of the average load, regardless of the cyclic loading direction; for the L-shaped

test, this is at approximately 45° to the I-direction as equal average load is applied in the I- and II-directions.

Figure 10 presents the monopile's ratcheting response in the I-direction for the T-shaped tests and in both the I- and II-direction for the L-shaped tests. The ratcheting responses for the corresponding unidirectional tests are also plotted. The ratcheting magnitude and evolution for the perpendicular tests is broadly similar to that under corresponding unidirectional loading, suggesting that ratcheting is approximately independent of the cycling loading direction for a given cyclic amplitude and average load. For the L-shape tests, the ratcheting magnitude perpendicular to the cycling direction (I) is smaller than that aligned with the cycling direction (II) in both the very loose and dense samples, suggesting some non-linear dependency of ratcheting on load magnitude.

These results show how ratcheting is aligned to the direction of average load, and suggest that – to a first approximation – the magnitude of ratcheting may be considered independent of the cyclic loading direction. These observations have important implications for modelling the multidirectional cyclic response; ratcheting in the direction of the applied load is a key feature of, for instance, the HARM modelling approach (Houlsby *et al.*, 2017), and may be included as a feature of explicit ratcheting models.

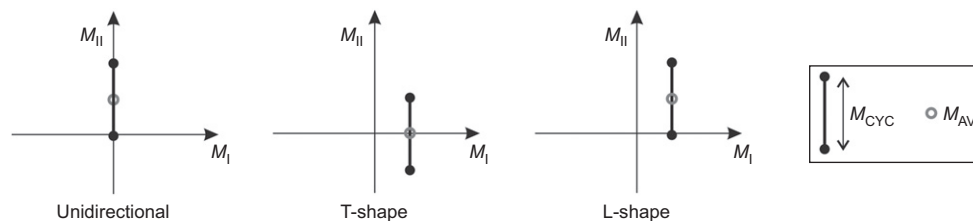


Fig. 8. Schematic representation of perpendicular loading cases

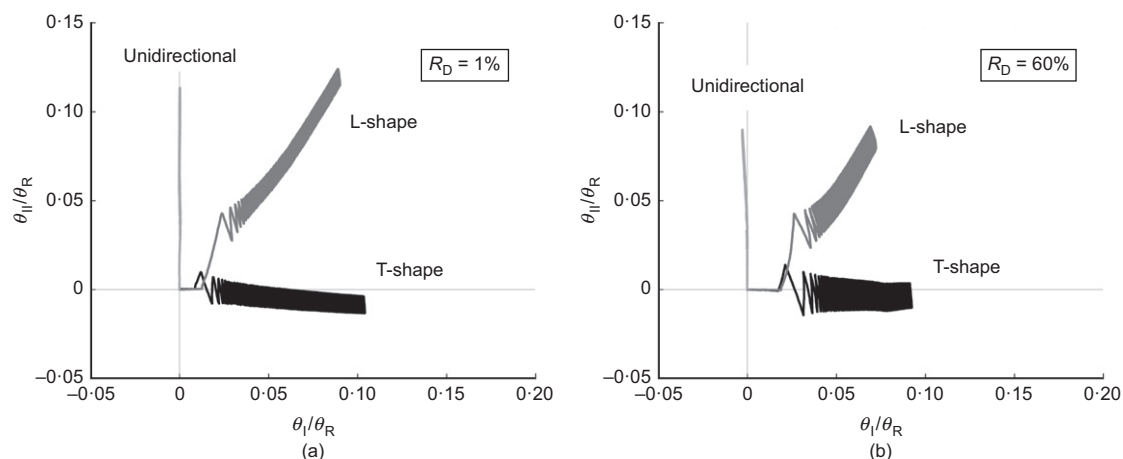


Fig. 9. Total rotation response for perpendicular loading tests: (a) very loose sample; (b) dense sample

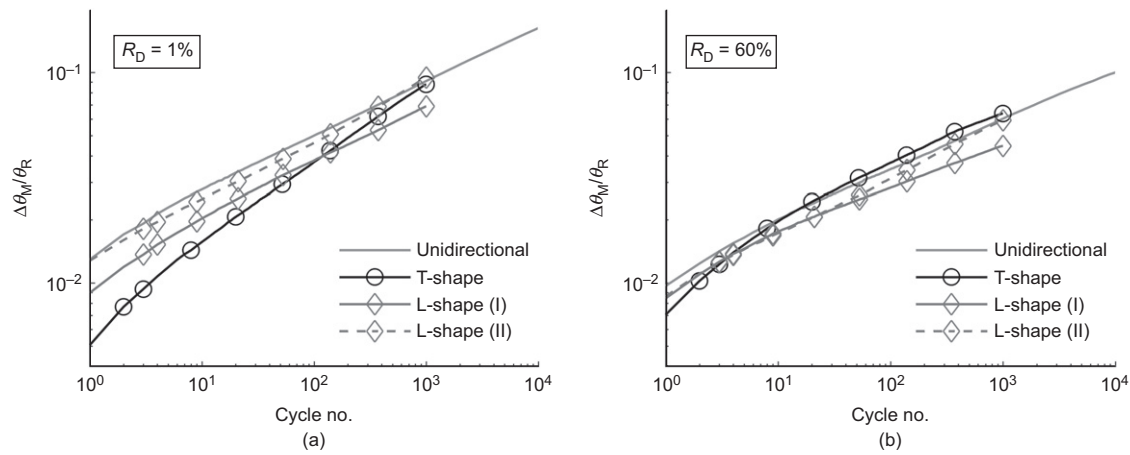


Fig. 10. Ratcheting response under perpendicular cyclic loading: (a) very loose sample; (b) dense sample

Table 6. Fan-type loading test series

Test name	Corresponding unidirectional test	Sand density	Spread angle, Φ	ζ_b	ζ_c	Cycles, N
L.F1	L.C3	Very loose	15°	0.40	0	1000
L.F2	L.C3	Very loose	30°	0.40	0	1000
L.F3	L.C3	Very loose	45°	0.40	0	1000
L.F4	L.C3	Very loose	60°	0.40	0	1000
L.F5	L.C3	Very loose	90°	0.40	0	1000
L.F6	L.C3	Very loose	120°	0.40	0	1000
L.F7	L.C3	Very loose	150°	0.40	0	1000
D.F1	D.C3	Dense	30°	0.20	0	1000
D.F2	D.C3	Dense	90°	0.20	0	1000

Fan-type loading

Table 6 summarises the fan-type loading tests performed, and Fig. 11 demonstrates the loading applied to the monopile for the example case of D.F1. In M_I – M_{II} space the loading traces the sector of a circle with radius $\zeta_b M_R$ and half internal angle Φ , which is referred to as the spread angle. The loading direction varies sinusoidally at a frequency $1/100$ of the cyclic loading frequency, f_c , so 1000 cycles corresponds to ten complete sweeps of the sector. Equations (6)–(8) define the M_I and M_{II} direction loads, while Fig. 11 also shows the example M_I and M_{II} loading for half a sweep.

$$A(t) = \frac{M_R \zeta_b}{2} [1 + \sin(2\pi f_c t)] \quad (6)$$

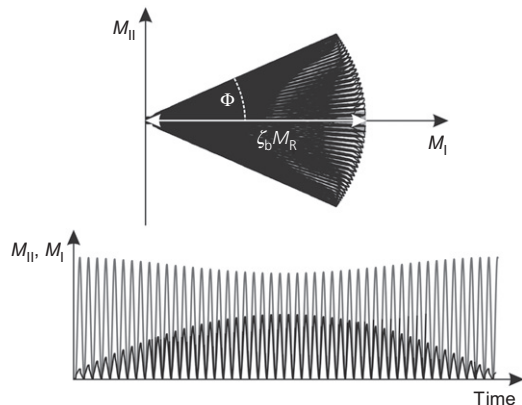


Fig. 11. Schematic representation of fan-type loading

$$M_I = A(t) \cos \left[\Phi \sin \left(\frac{2\pi f_c t}{100} \right) \right] \quad (7)$$

$$M_{II} = A(t) \sin \left[\Phi \sin \left(\frac{2\pi f_c t}{100} \right) \right] \quad (8)$$

Figure 12 shows the evolution of the magnitude of ratcheting for the tests summarised in Table 6, alongside the corresponding unidirectional response ($\Phi = 0^\circ$). For the fan tests, the rate of change of ratcheting varies as the loading angle changes, seen as ‘ripples’ in the ratcheting evolution. The magnitude of these ripples increases with increasing multidirectionality. Similar behaviour is observed in the very loose and dense samples.

The impact of spread angle on overall ratcheting rate can be assessed by finding the change in exponent α with Φ . Equation (5) is fitted to each of the ten fan-type tests, fixing the intercept A to the value of A for the corresponding unidirectional test. A is not expected to vary with Φ , as loading is close to unidirectional during the first few cycles. The fits are shown for the fan-type tests in Fig. 12, whilst the variation of α with spread angle Φ is shown in Fig. 13. There is a clear dependency of exponent α on spread angle Φ , with peak exponent amplification (worst case) occurring at $\Phi = 90^\circ$ for both very loose and dense sand. The dependency is less pronounced in the dense sand than in the very loose sand, although the trend is similar.

The impact of spread angle can also be assessed with the ratio of displacement at cycle N under multidirectional loading to that under equivalent unidirectional loading. This multidirectional factor is summarised for the worst-case spread angles for this study and similar studies in Table 7.

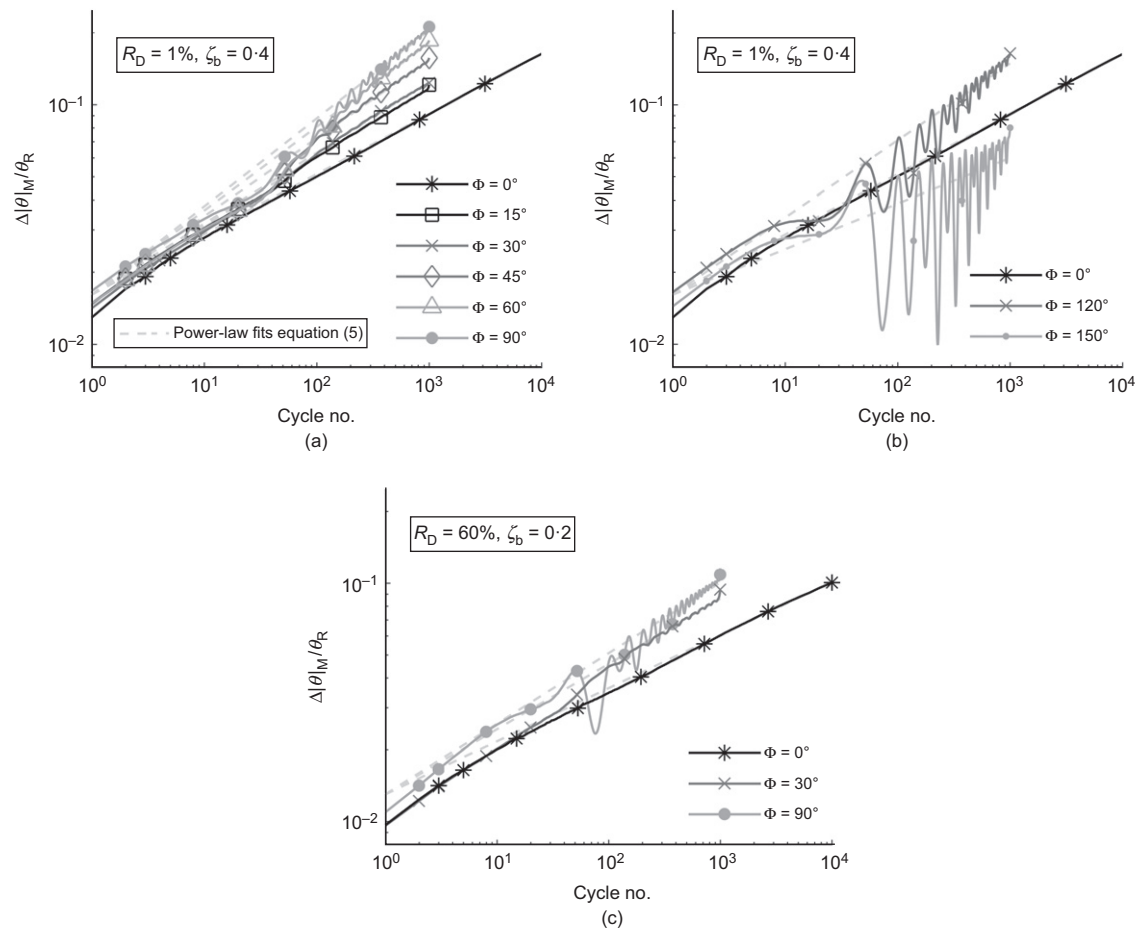


Fig. 12. Ratcheting response under multidirectional fan-type loading: (a) very loose sample, low Φ ; (b) very loose sample, high Φ ; (c) dense sample

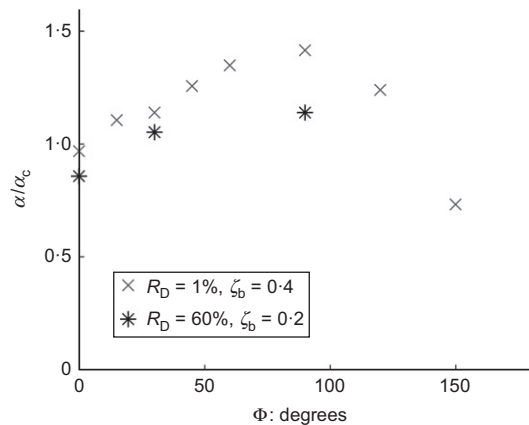


Fig. 13. Variation of α with spread angle Φ for fan-type tests

Although an increase in pile displacement under spread cyclic loading is observed in all studies, there is significant variation in multidirectional factor and worst-case spread angle.

The applied loading pattern will be critical for the observed ratcheting behaviour, and the worst-case spread angle and multidirectional factor are likely to vary with specific load regime, as reported by Rudolph *et al.* (2014a). Direct application of a multidirectional factor is therefore not recommended, but these results highlight the need to account for multidirectionality to ensure conservative design.

Similarly to partial two-way loading, the impact of increasing spread angle on the ratcheting behaviour may be understood qualitatively as a competition between increasing pile and therefore soil movement and a decreasing mean load in the dominant loading direction.

Table 7. Factors on unidirectional displacement from multidirectional fan-type studies

Study	Displacement metric	Laboratory conditions	Cycles, N	Worst-case spread angle, Φ	Multidirectional factor
Dührkop & Grabe (2008)	Pile head displacement	1g, medium-dense sand	50 000	45°	1.3
Rudolph <i>et al.</i> (2014b)	Displacement at lowest LVDT	1g, dense sand	50 000	45°	2–3
		1g, medium-dense sand	10 000	90°	1.2
		1g, dense sand	10 000	120°	1.4
		200g, medium-dense sand	3000	30°	1.7
		200g, dense sand	3000	90°	1.5
Present study	Accumulated pile rotation	1g, very loose sand	1000	90°	2.3
		1g, dense sand	1000	90°	1.8

RELOADING RESPONSE

Reloading tests to $\sim 0.8M_R$ were performed to explore the post-cyclic capacity of the monopile, which is of great importance for ULS design. Understanding the monopile's post-cyclic response also informs interpretation of multi-amplitude loading. Fig. 14 shows the post-cyclic response of tests in Tables 4 and 6 (except test L.C1 where reloading was not performed). The cyclic response is omitted from the plots for clarity, and the undisturbed monotonic response (backbone curve) is plotted dashed for comparison.

All reloading responses exhibit a higher stiffness in the cyclic loading region, relative to the backbone curve, shown clearly when the reloading responses are re-zeroed (Figs 14(c) and 14(d)). In many cases, the total reloading curve (Figs 14(a) and 14(b)) crosses the backbone curve, indicating a true increase in capacity. In other cases – particularly where significant ratcheting has occurred – the reloading test has not been displaced enough to reach the backbone curve. However, these tests clearly approach the backbone curve and would either meet or cross the backbone curve given sufficient rotation. Although the total reloading curves indicate a greater increase in capacity for the dense sand, on average less ratcheting occurs for the dense tests presented. With the reloading responses re-zeroed the behaviour is qualitatively similar at both densities.

Truong *et al.* (2019) and Nicolai *et al.* (2017) also report an increase in post-cyclic monotonic capacity, and Nicolai *et al.* (2017) are further able to quantify the increase in capacity in terms of cycle number, ζ_c and ζ_b , given that their reloading

tests reach clear yield. The increase in post-cyclic capacity in sand is also likely to be caused by the same mechanisms that lead to an increase in secant stiffness with cyclic loading, as observed in other studies (Leblanc *et al.*, 2010a; Abadie, 2015; Truong *et al.*, 2019).

Established approaches for designing piles for cyclic lateral loading in sand apply reduction factors to derived p – y curves to reduce the pile's lateral capacity (e.g. Murchison & O'Neill, 1984). However, the current experimental evidence does not support a decrease in post-cyclic capacity in dry (fully drained) sands, and indeed an increase in capacity is often observed, which may be exploited to optimise monopile design.

REALISTIC STORM LOADING

The constant-amplitude tests presented in previous sections allow systematic investigation of the monopile's response. In practice, however, foundations experience environmental loading which continually varies in amplitude, frequency and direction. The tests presented in this section – with loading derived from wave tank experiments – highlight salient features of the foundation's response to realistic loading and are useful for model validation and verification. These tests therefore complement the constant-amplitude tests.

Tests have only been conducted in very loose sand in this section, but given the consistent behaviour between densities reported in the previous sections of this paper, qualitatively similar behaviour may be expected in dense sand.

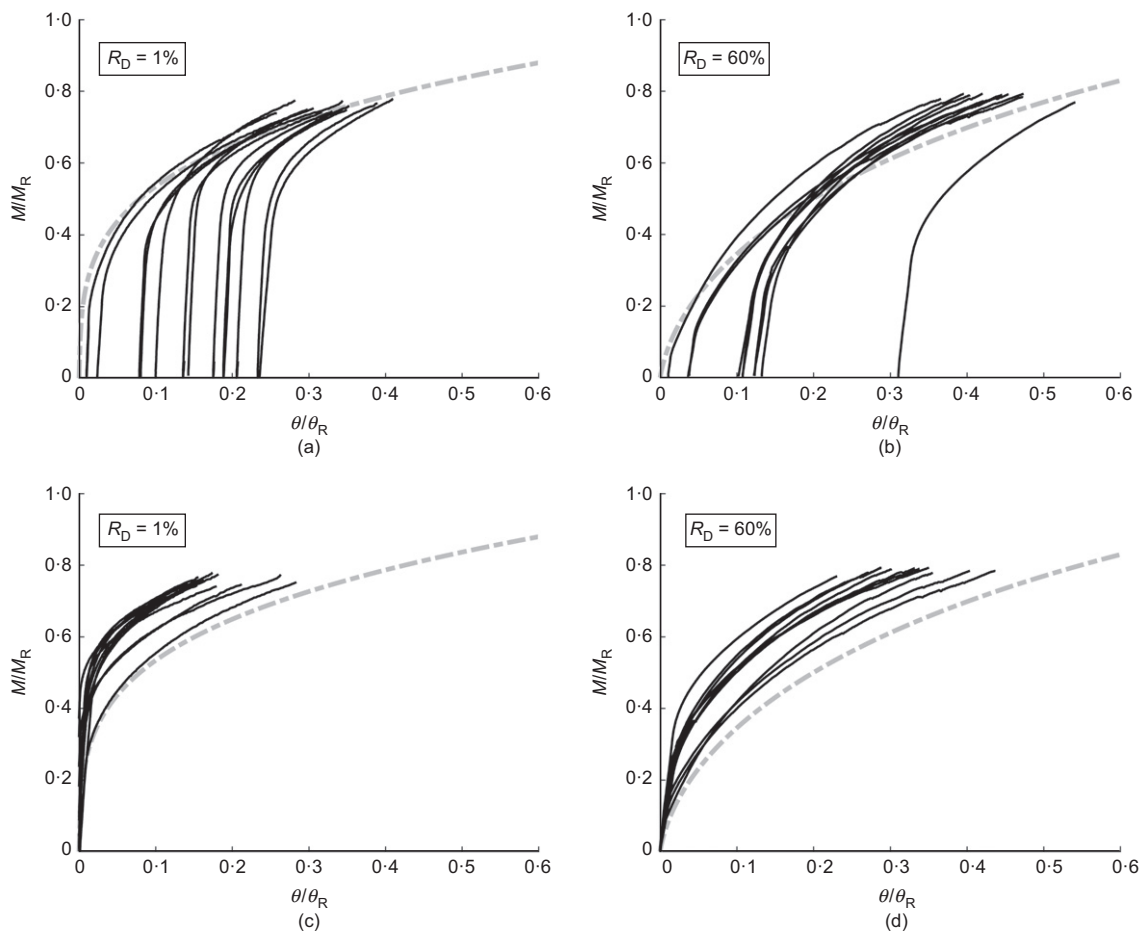


Fig. 14. Reloading response: (a) very loose sample, total rotation on reloading; (b) dense sample, total rotation on reloading; (c) very loose sample, rotation zeroed from onset of reloading; (d) dense sample, rotation zeroed from onset of reloading (monotonic response shown dashed)

Wave tank experiments

A number of model-scale wave loading tests were performed at the Danish Hydraulic Institute (DHI) to explore wave–structure interaction as part of the DeRisk project, a large multi-centre research project aimed at reducing the risk associated with predicting ULS wave loads on OWT structures (Bredmose *et al.*, 2016). The DeRisk tests were performed at 1:50 scale in a shallow water basin. The monopile was modelled as a stiff cylinder of diameter 140 mm, instrumented with (among other instruments) four load cells to allow resolution of the total horizontal and moment load applied to the cylinder. A range of wave conditions were generated, representative of large waves in severe storms in the North Sea. Both unidirectional and directionally spread sea states were investigated (Bredmose *et al.*, 2016).

Generation of model-scale loads

The tests presented in this paper have been derived from two DeRisk wave tests: a unidirectional test (UD95) and a multidirectional test (MD95). These wave tests were conducted in the equivalent of 33 m water depth with peak spectral period 15 s and significant wave height 9.5 m at prototype scale. The multidirectional sea state has a spreading angle of 22°. Measured loads (H_I , H_{II} , M_I , M_{II}) on the cylinder were provided at prototype scale, and a number of basic processing steps were performed before applying the loads to the model monopile: (a) addition of constant wind loading; (b) application of a transfer function to model the structure's dynamic response; (c) projection of loads to constant eccentricity; (d) scaling to model scale.

To represent real loading on an OWT, the measured wave loads are combined with wind loading, approximated as a constant force. Given the large significant wave height in the DeRisk tests, the turbine is assumed to be in a parked condition in an extreme storm. A wind load of 1.4 MN acting at a height 85.5 m above the mudline (120 MN m) is estimated, assuming appropriate OWT dimensions and a 50 year design wind speed of 50 m/s. Wind loading is aligned with the dominant wave loading direction.

A transfer function is applied to the loads to capture the dynamic response of the OWT structure. This process is necessary as the DeRisk tests were performed on a very stiff cylinder, with no dynamic amplification of loads. The OWT

structure is approximated as a single-degree-of-freedom system with a natural frequency f_0 and damping ratio ξ . For such a system the ratio of transmitted force F to excitation force P can be found as

$$\frac{F}{P} = \frac{1}{\sqrt{[1 - (f/f_0)^2]^2 + [2\xi(f/f_0)]^2}} \quad (9)$$

This simple transfer function is thought to capture the OWT's key dynamic behaviour, and has been used by, for example, Arany *et al.* (2017). The prototype structure's first natural frequency is estimated as $f_0 = 0.26$ Hz, between the 1P and 3P excitation frequencies for a Vestas V164-8.0 MW turbine (ESRU, 2015). Estimating the damping coefficient is more difficult, as there is much variation in values reported in the literature, and damping varies with turbine operation conditions (Devriendt & Weijtjens, 2015). For parked conditions, where aerodynamic damping is negligible, the total damping is estimated as $\xi = 0.65\%$, in line with Kementzetzidis *et al.* (2019) for dense sand.

This transfer function (equation (9)) is approximated by an arbitrary magnitude digital filter and applied to the load signals in the frequency domain using Matlab function 'filter'. Fig. 15(a) shows the significant impact of the transfer function on the moment (M_I) transmitted to the foundation for 100 s of signal at prototype scale, for the example case of test MD95 with additional constant wind loading.

Next, the loads are projected to a constant load eccentricity (M/H), as shown in Fig. 15(b) for the example case of tests MD95 with wind loading. This is necessary as the measured wave loads have a variable load eccentricity, but the laboratory apparatus can only apply loads at a single eccentricity. Loads are projected onto a 'load line' in M – H space, with gradient equivalent to the fixed loading eccentricity of the laboratory apparatus, in a direction parallel to a monopile yield surface. An approximate expression for a monopile yield surface is obtained by assuming a distributed lateral load per unit length of $DK\gamma'z$, taking $K = 3K_p$ (Broms, 1964) with $\phi' = 40^\circ$ and linearising the yield surface in the region of interest (where M/H is positive)

$$M/(L^3 D\gamma') + 0.75H/(L^2 D\gamma') = 0.29K_p \quad (10)$$

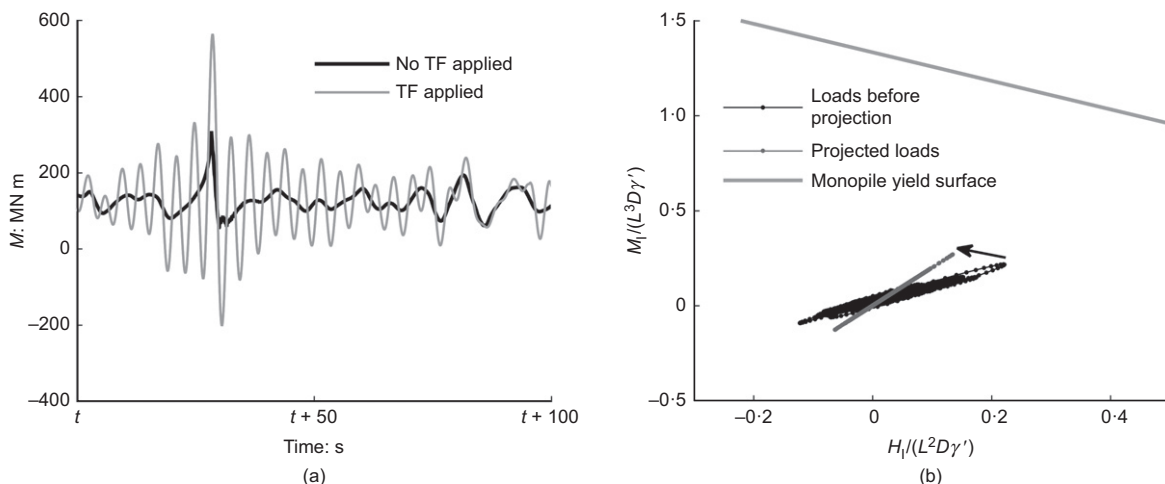


Fig. 15. Processing DeRisk load data for the example case of test MD95 with wind loading: (a) impact of transfer function (TF) on M_I ; (b) demonstration of projection of I-direction wave loads to constant eccentricity

Table 8. Storm loading test series

Test name	Sand density	Source DeRisk test	Directionality	Wind load	I-direction		II-direction	
					M_{MAX}/M_R	M_{AV}/M_R	M_{MAX}/M_R	M_{AV}/M_R
L.DR1	Very loose	UD95	Unidirectional	N	0.40	0.00	0.00	0.00
L.DR2	Very loose	UD95	Unidirectional	Y	0.46	0.07	0.00	0.00
L.DR3	Very loose	MD95	Multidirectional	N	0.47	0.00	0.13	0.00
L.DR4	Very loose	MD95	Multidirectional	Y	0.53	0.07	0.13	0.00
L.DR5	Very loose	MD95	Unidirectional	N	0.47	0.00	0.00	0.00
L.DR6	Very loose	MD95	Unidirectional	Y	0.53	0.07	0.00	0.00

For multidirectional loading, the I- and II-direction components are projected independently.

Finally, the processed prototype-scale loads are translated to model scale using the dimensionless framework presented in Table 3. The prototype monopile is assumed to have diameter $D = 8$ m and length $L = 32$ m, which may be appropriate for very loose sand. The prototype soil unit weight is estimated as $\gamma' = 10$ kN/m³, given that it would be saturated.

Table 8 summarises the storm loading tests presented in this paper. All tests include approximately 5000 load cycles (with the transfer function applied) and are derived from either DeRisk test UD95 or MD95. The maximum normalised load M_{MAX}/M_R (equivalent to ζ_b) varies from 0.40 to 0.53 across the test series. Wind loading is added to alternate cases, increasing the average normalised moment to produce overall partial two-way loading ($M_{AV}/M_R > 0$), consistent with the findings of Jalbi *et al.* (2019) for extreme storm loading in deep waters.

Tests L.DR5 and L.DR6 are unidirectional (UD) versions of the multidirectional (MD) tests L.DR3 and L.DR4, respectively; only the dominant I-direction component of loading is applied in these tests, as demonstrated in Fig. 16 for L.DR6 and L.DR4.

Figure 17 presents the distribution of M_{CYC}/M_R and M_{AV}/M_R (and equivalently ζ_b and ζ_c) considering each half-cycle, for the example case of test L.DR4 (corresponding to wave test MD95 with wind loading) in the I-direction. The majority of the loading occurs at $\zeta_b < 0.25$, with the largest amplitude cycles partially two-way ($-1 < \zeta_c < 0$).

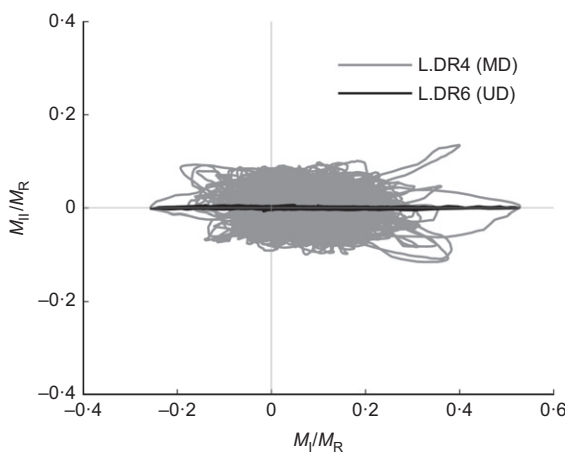


Fig. 16. Comparison of multidirectional and unidirectional loads, for the example cases of L.DR4 and L.DR6

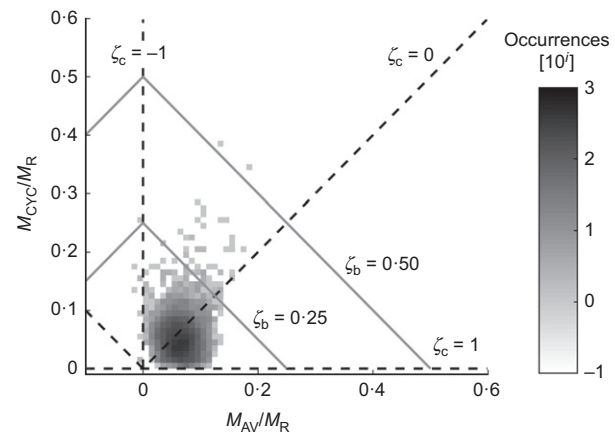


Fig. 17. Distribution of M_I loads for example case of test L.DR4

Monopile response

The response of the monopile to the storm loading is presented in Fig. 18. For the multidirectional tests, only the behaviour in the direction of dominant loading (I-direction) is presented. The moment–rotation plots show the foundation's hysteretic response, while the foundation's total rotation with cycle number is used to present the ratcheting behaviour. Some stiffening can be observed in the moment–rotation plots, but is not discussed further here.

In general, the increase in pile rotation is dominated by the large load events – as seen in both the moment–rotation plots and the ratcheting evolution plots. The moment–rotation plots also show how the response generally follows the backbone curve (shown grey dashed) when loads exceed those previously applied, broadly aligned with observations from constant-amplitude reloading tests. The maximum rotation during a short storm may, therefore, be approximated by the monotonic response.

Tests L.DR1 and L.DR2, and tests L.DR3 and L.DR4 are each derived from the same DeRisk load signals, but L.DR2 and L.DR4 have an additional wind loading bias. The impact of the load bias is clear, with greater ratcheting recorded for L.DR2 and L.DR4 than L.DR1 and L.DR3, respectively.

Comparing tests L.DR3 and L.DR5, and L.DR4 and L.DR6 provides insight into the impact of multidirectional loading. Fig. 17 shows a slight increase in total rotation at a given cycle number for the multidirectional cases (L.DR3 and L.DR4), with the increase in total rotation increasing with cycle number. These results are broadly consistent with the behaviour under constant-amplitude fan-type loading at small fan angles ($\Phi < 30^\circ$).

Overall, these tests provide insight into the monopile's response to realistic multi-amplitude, multidirectional

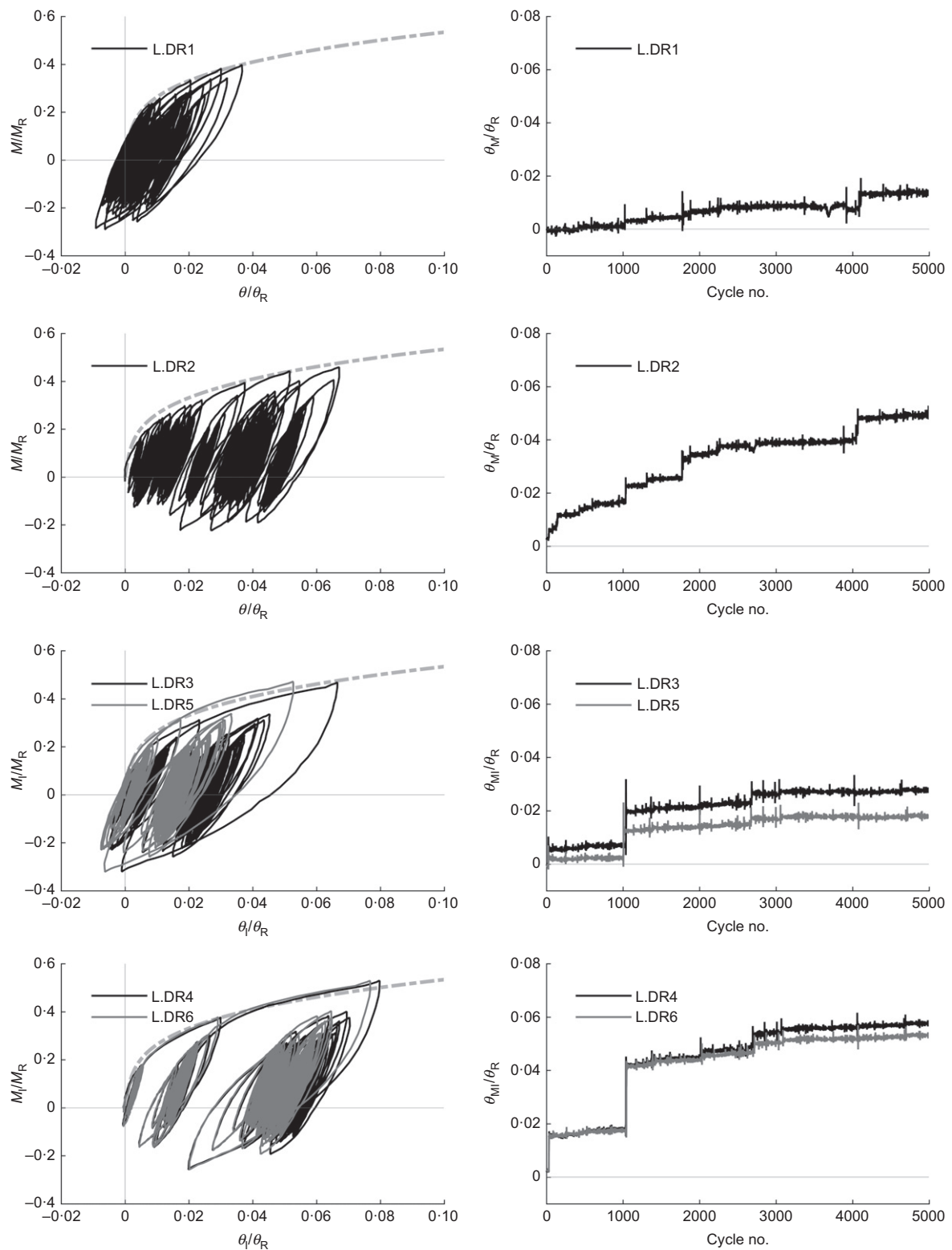


Fig. 18. Response to storm loading in dominant (I) loading direction (monotonic response shown dashed)

loading, and importantly show behaviour that is consistent with the previous constant-amplitude tests.

CONCLUSIONS

This paper has presented results from cyclic lateral loading tests on a laboratory-scale monopile foundation in dry sand at 1g. The results are consistent with previous experimental studies, and provide new insights in terms of the response

of the monopile to perpendicular cyclic loading and realistic multi-amplitude and multidirectional cyclic loading. The following key observations are made.

- (a) The rotation response in very loose and dense, dry sand is qualitatively similar, increasing confidence in the application of theoretical models developed for very loose sands (e.g. Abadie *et al.*, 2017) to denser material typically encountered offshore.

- (b) Partial two-way loading can cause greater ratcheting than one-way loading to the same peak load, and multidirectional fan-type loading can cause greater ratcheting than unidirectional loading to the same peak load.
- (c) Ratcheting occurs in the direction of load bias, and is largely unaffected by the cyclic loading direction; this observation has important implications for theoretical modelling.
- (d) Monopile capacity is either maintained or increased following cyclic loading in dry (fully drained) sand, at odds with the idea that cyclic loading is always a damaging process.
- (e) The response to realistic multi-amplitude, multidirectional storm-type loading is consistent with observations from constant-amplitude tests.
- (f) The maximum rotation during a short storm in dry (drained) sand may be approximated by the monotonic response.

Because great care is necessary in scaling laboratory-scale responses to full scale, and the process is subject to uncertainties, these results should not be directly applied for full-scale design. Nevertheless, these patterns of behaviour are broadly consistent with those observed under unidirectional cyclic loading at large field scale (Beuckelaers, 2017), and are therefore expected to translate to full scale. These results can inform development of models, such as HARM; specifically, the constant-amplitude results can be used for model calibration, while the realistic loading tests aid validation. Of course, before application for full-scale design, such a model would need to be developed to account for scaling effects and validated at full scale.

ACKNOWLEDGEMENTS

This work was supported by grant EP/L016303/1 for Cranfield University, the University of Oxford and Strathclyde University, Centre for Doctoral Training in Renewable Energy Marine Structures (REMS, <http://www.rems-cdt.ac.uk/>) from the UK Engineering and Physical Sciences Research Council (EPSRC). The storm loading data used in this paper came from the DeRisk project, funded by Innovation Fund Denmark.

The research materials supporting this publication can be accessed by contacting byron.byrne@eng.ox.ac.uk.

NOTATION

A	fitting parameter
D	pile diameter
$D_{10}, D_{30}, D_{50}, D_{60}$	soil particle sizes
\tilde{e}	dimensionless loading eccentricity
F	transmitted force
f_0	natural frequency
f_c	cyclic loading frequency
H	horizontal load
\tilde{H}	dimensionless horizontal load
h	pile loading eccentricity
K_p	coefficient of passive earth pressure
L	pile embedded length
M	moment load
\tilde{M}	dimensionless moment load
M_{AV}	average moment load
M_{CYC}	cyclic moment load
M_D	design moment load
M_{MAX}	maximum moment load
M_{MIN}	minimum moment load
M_R	reference moment load
N	cycle number
P	excitation force

p_a	atmospheric pressure
R_a	average surface roughness
R_D	relative density
t	pile wall thickness
γ'	effective unit weight
γ'_{MAX}	maximum unit weight
γ'_{MIN}	minimum unit weight
$\Delta\theta$	accumulated pile rotation (per cycle)
$\Delta\theta_M$	accumulated mean pile rotation (per cycle)
ε	strain
ζ_b	load amplitude characterisation parameter
ζ_c	load symmetry characterisation parameter
θ	pile rotation
$\tilde{\theta}$	dimensionless pile rotation
θ_D	design rotation
θ_M	total mean pile rotation (per cycle)
θ_R	reference pile rotation
θ_{RL}	pile reloading rotation
ζ	damping ratio
σ'_v	vertical effective stress
Φ	spread angle
ϕ'	friction angle
ϕ'_{cr}	critical friction angle
ϕ'_p	peak friction angle

REFERENCES

- Abadie, C. N. (2015). *Cyclic lateral loading of monopile foundations in cohesionless soils*. DPhil thesis, University of Oxford, Oxford, UK.
- Abadie, C. N., Byrne, B. W. & Houlsby, G. T. (2017). Modelling of monopile response to cyclic lateral loading in sand. In *Proceedings of the 8th international conference on offshore site investigation and geotechnics*, pp. 1046–1053. London, UK: Society for Underwater Technology.
- Abadie, C. N., Byrne, B. W. & Houlsby, G. T. (2019a). Rigid pile response to cyclic lateral loading: laboratory tests. *Géotechnique* **69**, No. 10, 863–876, <https://doi.org/10.1680/jgeot.16.P325>.
- Abadie, C. N., Houlsby, G. T. & Byrne, B. W. (2019b). A method for calibration of the hyperplastic accelerated ratcheting model (HARM). *Comput. Geotech.* **112**, 370–385.
- Achmus, M., Abdel-Rahman, K. & Kuo, Y. (2007). Numerical modelling of large diameter steel piles under monotonic and cyclic horizontal loading. In *Proceedings of 10th international symposium on numerical models in geomechanics* (eds G. N. Pande and S. Pietruszczak), pp. 453–460. London, UK: CRC Press.
- Achmus, M., Kuo, Y. S. & Abdel-Rahman, K. (2009). Behavior of monopile foundations under cyclic lateral load. *Comput. Geotech.* **36**, No. 5, 725–735.
- Albiker, J., Achmus, M., Frick, D. & Flindt, F. (2017). 1g model tests on the displacement accumulation of large-diameter piles under cyclic lateral loading. *Geotech. Testing J.* **40**, No. 2, 173–184.
- Altaee, A. & Fellenius, B. H. (1994). Physical modeling in sand. *Can. Geotech. J.* **31**, No. 3, 420–431.
- Andersen, K. H. (2015). Cyclic soil parameters for offshore foundation design. In *Frontiers in offshore geotechnics III* (ed. V. Meyer), pp. 3–82. Leiden, the Netherlands: CRC Press/Balkema.
- API (American Petroleum Institute) (2011). *Geotechnical and foundation design considerations ANSI/API RP 2GEO*. Washington, DC, USA: API.
- Arany, L., Bhattacharya, S., Macdonald, J. & Hogan, S. J. (2017). Design of monopiles for offshore wind turbines in 10 steps. *Soil Dynamics Earthquake Engng* **92**, 126–152.
- Arshad, M. & O'Kelly, B. C. (2017). Model studies on monopile behavior under long-term repeated lateral loading. *Int. J. Geomech.* **17**, No. 1, 1–12.
- Bayton, S. M., Black, J. A. & Klinkvort, R. T. (2018). Centrifuge modelling of long term cyclic lateral loading on monopiles. In *Physical modelling in geotechnics – ICPMG 2018* (eds A. McNamara, S. Divall, R. Goodey, N. Taylor, S. Stallebrass and J. Panchal), pp. 689–694. London, UK: CRC Press.
- Beuckelaers, W. J. A. P. (2017). *Numerical modelling of laterally loaded piles for offshore wind turbines*. DPhil thesis, University of Oxford, Oxford, UK.

- Bierbooms, W. (2003). *Wind and wave conditions, DOWEC (Dutch Offshore Wind Energy Converter Project)*. Delft University of Technology, Delft, the Netherlands.
- Bolton, M. D. (1986). The strength and dilatancy of sands. *Geotechnique* **36**, No. 1, 65–78, <https://doi.org/10.1680/geot.1986.36.1.65>.
- Bolton, M. D. (1987). Discussion: the strength and dilatancy of sands. *Geotechnique* **37**, No. 2, 219–226, <https://doi.org/10.1680/geot.1987.37.2.219>.
- Bredmose, H., Dixen, M., Ghadirian, A., Larsen, T. J., Schløer, S. & Hanson, T. D. (2016). Derisk – accurate prediction of ULS wave loads. Outlook and first results. *Energy Procedia* **94**, 379–387.
- Broms, B. B. (1964). Lateral resistance of piles in cohesionless soils. *ASCE J. Soil Mech. Found. Div.* **90**, No. May, 123–156.
- Byrne, B. W., McAdam, R. A., Burd, H. J., Houlsby, G. T., Martin, C. M. & Plummer, M. A. L. (2017). PISA: new design method for offshore wind turbine monopiles. In *Proceedings of the 8th international conference on offshore site investigation and geotechnics*, vol. 1, pp. 142–161. London, UK: Society for Underwater Technology.
- Cuéllar, V. P. (2011). *Pile foundations for offshore wind turbines: numerical and experimental investigations on the behaviour under short-term and long-term cyclic loading*. PhD thesis, Technischen Universität, Berlin, Germany.
- Devriendt, C. & Weijtjens, W. (2015). The overall damping of an offshore wind turbine during different operating conditions. *EWEA (European Wind Energy Association) offshore 2015*, Copenhagen, Denmark.
- DNV GL (2016). *DNVGL-ST-0126: Support structures for wind turbines (April ed.)*. Oslo, Norway: DNV GL.
- Dührkop, J. & Grabe, J. (2008). Monopilegründungen von Offshore-windenergieanlagen – zum Einfluss einer veränderlichen zyklischen Lastangriffsrichtung. *Bautechnik* **85**, No. 5, 317–321 (in German).
- ESRU (The Energy Systems Research Unit) (2015). *XL monopiles*. Glasgow, UK: University of Strathclyde, see http://www.esru.strath.ac.uk/EandE/Web_sites/14-15/XL_Monopiles/structural.html (accessed 30/10/2018).
- Houlsby, G. T., Abadie, C. N., Beuckelaers, W. J. A. P. & Byrne, B. W. (2017). A model for nonlinear hysteretic and ratcheting behaviour. *Int. J. Solids Structs* **120**, 67–80.
- Jalbi, S., Arany, L., Salem, A., Cui, L. & Bhattacharya, S. (2019). A method to predict the cyclic loading profiles (one-way or two-way) for monopile supported offshore wind turbines. *Mar. Structs* **63**, 65–83.
- Kementzetzidis, E., Corciulo, S., Versteijlen, W. G. & Pisanò, F. (2019). Geotechnical aspects of offshore wind turbine dynamics from 3D non-linear soil–structure simulations. *Soil Dynamics Earthquake Engng* **120**, 181–199.
- Klinkvort, R. (2012). *Centrifuge modelling of drained lateral pile–soil response*. PhD thesis, Technical University of Denmark, Lyngby, Denmark.
- Klinkvort, R. & Hededal, O. (2013). Lateral response of monopile supporting an offshore wind turbine. *Proc. Instn Civ. Engrs – Geotech. Engng* **166**, No. 2, 147–158, <https://doi.org/10.1680/geng.12.00033>.
- Lauder, K. & Brown, M. J. (2014). Scaling effects in the 1g modelling of offshore pipeline ploughs. In *Physical modelling in geotechnics – ICPMG 2014* (eds C. Gaudin and D. White), pp. 377–383. London, UK: CRC Press.
- Leblanc, C., Byrne, B. W. & Houlsby, G. T. (2010a). Response of stiff piles to random two-way lateral loading. *Geotechnique* **60**, No. 9, 715–721, <https://doi.org/10.1680/geot.09.T.011>.
- Leblanc, C., Houlsby, G. T. & Byrne, B. W. (2010b). Response of stiff piles in sand to long-term cyclic lateral loading. *Geotechnique* **60**, No. 2, 79–90, <https://doi.org/10.1680/geot.7.00196>.
- Murchison, J. M. & O'Neill, M. W. (1984). Evaluation of p – y relations in cohesionless soils. In *Proceedings of the ASCE symposium on analysis and design of pile foundations* (ed. J. R. Meyer), pp. 174–191. New York, NY, USA: American Society of Civil Engineers.
- Nicolai, G. (2017). *Cyclic behaviour of laterally loaded monopiles in sand supporting offshore wind turbines*. PhD thesis, Aalborg University, Aalborg, Denmark.
- Nicolai, G. & Ibsen, L. B. (2014). Small-scale testing of cyclic laterally loaded monopiles in dense saturated sand. *J. Ocean Wind Energy* **1**, No. 4, 240–245.
- Nicolai, G., Ibsen, L. B., O'Loughlin, C. D. & White, D. J. (2017). Quantifying the increase in lateral capacity of monopiles in sand due to cyclic loading. *Geotechnique Lett.* **7**, No. 3, 1–8, <https://doi.org/10.1680/jgele.16.00187>.
- Page, A. M., Grimstad, G., Eiksund, G. R. & Jostad, H. P. (2018). A macro-element pile foundation model for integrated analyses of monopile-based offshore wind turbines. *Ocean Engng* **167**, 23–35.
- Richards, I. A., Byrne, B. W. & Houlsby, G. T. (2018). Physical modelling of monopile foundations under variable cyclic lateral loading. In *Physical modelling in geotechnics – ICPMG 2018* (eds A. McNamara, S. Divall, R. Goodey, N. Taylor, S. Stallebrass and J. Panchal), pp. 737–742. London, UK: CRC Press.
- Rudolph, C. & Grabe, J. (2013). Untersuchungen zu zyklisch horizontal belasteten Pfählen bei veränderlicher Lastrichtung. *Geotechnik* **36**, No. 2, 90–95 (in German).
- Rudolph, C., Bienen, B. & Grabe, J. (2014a). Effect of variation of the loading direction on the displacement accumulation of large-diameter piles under cyclic lateral loading in sand. *Can. Geotech. J.* **51**, No. 10, 1196–1206.
- Rudolph, C., Grabe, J. & Bienen, B. (2014b). Drift of piles subjected to lateral loading from a varying direction: system vs. soil element behaviour. *Proceedings of ASME 2014 33rd international conference on ocean, offshore and arctic engineering*, San Francisco, CA, USA.
- Schnaid, F. (1990). *A study of the cone-pressuremeter test in sand*. DPhil thesis, University of Oxford, Oxford, UK.
- Schroeder, F. C., Merritt, A. S., Sørensen, K. W., Muir Wood, A., Thilsted, C. L. & Potts, D. M. (2015). Predicting monopile behaviour for the Gode wind offshore wind farm. In *Frontiers in offshore geotechnics III* (ed. V. Meyer), pp. 735–740. Leiden, the Netherlands: CRC Press/Balkema.
- Sørensen, S. P. H., Augustensen, A. H., Leth, C. T., Ostergaard, M. U. & Møller, M. (2017). Consequences of p – y curve selection for monopile design for offshore wind turbines. In *Proceedings of the 8th international conference on offshore site investigation and geotechnics*, vol. 2, pp. 1062–1069. London, UK: Society for Underwater Technology.
- Truong, P., Lehan, B. M., Zania, V. & Klinkvort, R. T. (2019). Empirical approach based on centrifuge testing for cyclic deformations of laterally loaded piles in sand. *Geotechnique* **69**, No. 2, 133–145, <https://doi.org/10.1680/jgeot.17.P.203>.
- Van Vledder, G. P. (2013). On wind-wave misalignment, directional spreading and wave loads. *Proceedings of the 32nd international conference on ocean, offshore and Arctic engineering OMAE2013*, Nantes, France.
- Wind Europe (2018). *Offshore wind in Europe: key trends and statistics 2017*. Brussels, Belgium: Wind Europe, see <https://windeurope.org/wp-content/uploads/files/about-wind/statistics/WindEurope-Annual-Offshore-Statistics-2017.pdf> (accessed 30/10/2018).
- Zhu, B., Byrne, B. W. & Houlsby, G. T. (2013). Long-term lateral cyclic response of suction Caisson foundations in sand. *J. Geotech. Geoenviron. Engng* **139**, No. 1, 73–83.
- Zhu, F. Y., O'Loughlin, C. D., Bienen, B., Cassidy, M. J. & Morgan, N. (2017). The response of suction caissons to long-term lateral cyclic loading in single-layer and layered seabeds. *Geotechnique* **67**, No. 11, 1–13, <https://doi.org/10.1680/jgeot.17.P.129>.